Published OnlineFirst October 17, 2014; DOI: 10.1158/1078-0432.CCR-14-1271

Cancer Therapy: Preclinical

Clinical Cancer Research

Systemic Delivery of Microencapsulated 3-Bromopyruvate for the Therapy of Pancreatic Cancer

Julius Chapiro[1], Surojit Sur[2], Lynn Jeanette Savic[1,3], Shanmugasundaram Ganapathy-Kanniappan[1], Juvenal Reyes[4], Rafael Duran[1], Sivarajan Chettiar Thiruganasambandam[4], Cassandra Rae Moats[5], MingDe Lin[1], Weibo Luo[6], Phuoc T. Tran[4], Joseph M. Herman[4], Gregg L. Semenza[6], Andrew J. Ewald[7], Bert Vogelstein[2], and Jean-François Geschwind[1]

Abstract

Purpose: This study characterized the therapeutic efficacy of a systemically administered formulation of 3-bromopyruvate (3-BrPA), microencapsulated in a complex with β-cyclodextrin (β-CD), using an orthotopic xenograft mouse model of pancreatic ductal adenocarcinoma (PDAC).

Experimental Design: The presence of the β-CD–3-BrPA complex was confirmed using nuclear magnetic resonance spectroscopy. Monolayer as well as three-dimensional organotypic cell culture was used to determine the half-maximal inhibitory concentrations (IC_{50}) of β-CD–3-BrPA, free 3-BrPA, β-CD (control), and gemcitabine in MiaPaCa-2 and Suit-2 cell lines, both in normoxia and hypoxia. Phase-contrast microscopy, bioluminescence imaging (BLI), as well as zymography and Matrigel assays were used to characterize the effects of the drug *in vitro*. An orthotopic *luc*MiaPaCa-2 xenograft tumor model was used to investigate the *in vivo* efficacy.

Results: β-CD–3-BrPA and free 3-BrPA demonstrated an almost identical IC_{50} profile in both PDAC cell lines with higher sensitivity in hypoxia. Using the Matrigel invasion assay as well as zymography, 3-BrPA showed anti-invasive effects in sublethal drug concentrations. *In vivo*, animals treated with β-CD–3-BrPA demonstrated minimal or no tumor progression as evident by the BLI signal as opposed to animals treated with gemcitabine or the β-CD (60-fold and 140-fold signal increase, respectively). In contrast to animals treated with free 3-BrPA, no lethal toxicity was observed for β-CD–3-BrPA.

Conclusion: The microencapsulation of 3-BrPA represents a promising step towards achieving the goal of systemically deliverable antiglycolytic tumor therapy. The strong anticancer effects of β-CD–3-BrPA combined with its favorable toxicity profile suggest that clinical trials, particularly in patients with PDAC, should be considered. *Clin Cancer Res; 20(24); 6406–17. ©2014 AACR.*

[1]Russell H. Morgan Department of Radiology and Radiological Science, Division of Vascular and Interventional Radiology, The Johns Hopkins University School of Medicine, Baltimore, Maryland. [2]Ludwig Center and Howard Hughes Medical Institute at the Johns Hopkins Kimmel Cancer Center, Baltimore, Maryland. [3]Department of Diagnostic and Interventional Radiology, Charité–Universitätsmedizin Berlin, Berlin, Germany. [4]Department of Radiation Oncology and Molecular Radiation Sciences, The Johns Hopkins University School of Medicine, Baltimore, Maryland. [5]Department of Molecular and Comparative Pathobiology, The Johns Hopkins University School of Medicine, Baltimore, Maryland. [6]Vascular Program, Institute for Cell Engineering and Department of Biological Chemistry, The Johns Hopkins University School of Medicine, Baltimore, Maryland. [7]Department of Cell Biology, The Johns Hopkins University School of Medicine, Baltimore, Maryland.

Note: Supplementary data for this article are available at Clinical Cancer Research Online (http://clincancerres.aacrjournals.org/).

J. Chapiro, S. Sur, and L.J. Savic contributed equally to this article.

Corresponding Author: Jean-François Geschwind, Johns Hopkins University, Sheikh Zayed Tower, Suite 7203, 1800 Orleans Street, Baltimore, MD 21287. Phone: 410-614 -6597; Fax: 410-955-0233; E-mail: jfg@jhmi.edu

doi: 10.1158/1078-0432.CCR-14-1271

Introduction

Pancreatic ductal adenocarcinomas (PDAC) rank as the fourth most common cause of cancer-related deaths in the world (1). As the majority of patients are diagnosed at advanced stages, therapeutic options remain limited and the prognosis is dismal, with a 5-year survival rate of less than 5% (2). The last two decades brought significant advances in the understanding of pancreatic tumorigenesis (2, 3). Pancreatic tumor tissue is composed of several distinctive, cellular, and noncellular elements including a collagen-rich, poorly vascularized and highly hypoxic, non-neoplastic stroma (4, 5). These characteristics are associated with chemoresistance to the most commonly used systemically applicable anticancer agents (6, 7). The distinctive tumor microenvironment is also commonly associated with altered tumor cell metabolism that is now recognized as a "hallmark" of the tumorigenic state (3, 8). The oxygen-independent reliance on glycolysis as the main axis of energy supply for cancer cells (and a subset of normal cells)

Published OnlineFirst October 17, 2014; DOI: 10.1158/1078-0432.CCR-14-1271

Translational Relevance

Selectively targeting tumor metabolism in pancreatic cancer has long been considered as a desirable therapeutic option but it has not yet been translated into clinical practice. The primary limitation in reaching the milestone of systemic deliverability of the antiglycolytic drug 3-bromopyruvate (3-BrPA) is the reported toxicity due to its alkylating properties. In this study, we characterized the therapeutic efficacy of a systemically administrable formulation of 3-BrPA, microencapsulated into a complex with β-cyclodextrin (β-CD). This novel formulation was developed and tested *in vitro* as well as *in vivo* using an orthotopic xenograft mouse model of pancreatic cancer. The main finding of this study is that systemically delivered β-CD–3-BrPA achieved strong antitumoral effects *in vivo* while causing much less toxicity in therapeutic doses when compared with the free drug. The results of this study suggest that clinical trials, particularly in patients with PDAC, should be considered.

has long been known as the "Warburg effect"; however, this effect has not yet been clinically exploited for therapeutic purposes (9, 10). 3-Bromopyruvate (3-BrPA), a highly potent small-molecular inhibitor of the enzyme GAPDH, represents the only available antiglycolytic drug candidate that is able to enter cancer cells selectively through the monocarboxylate transporter 1 (MCT1; refs. 11, 12). The antitumoral effects of 3-BrPA have been extensively studied in murine tumor models in the setting of locoregional therapy, delivered either through tumor-feeding arteries or with direct intratumoral injections (13, 14). However, due to its alkylating properties, 3-BrPA is associated with significant toxicity when delivered systemically in therapeutic doses, which has impeded the clinical development and use of this drug in patients with cancer (15, 16). Thus, there is a clear need to develop a new formulation of 3-BrPA with the capacity for systemic administration.

In the current study, we characterized the therapeutic efficacy of such a systemically administrable formulation of 3-BrPA, microencapsulated into a complex with β-cyclodextrin (β-CD). This novel formulation was developed and tested *in vitro* as well as *in vivo* using an orthotopic xenograft mouse model of pancreatic cancer.

Materials and Methods

In vitro studies

Antibodies, reagents, and kits. Following materials were used: Primary antibodies: rabbit anti-MMP-9 polyclonal antibody (pAb) #3852 (Cell Signaling Technology), DAPI #D1306 (Invitrogen), Alexa Fluor 568 Phalloidin #12380 (Life Technologies), GAPDH (14C10) monoclonal antibody Alexa Fluor 488 conjugate #3906 (Cell Signaling Technology), GAPDH pAb #sc-47724 (Santa Cruz Biotechnology), cleaved caspase-3 pAb #9661 (Cell Signaling Technology), MCT-1 pAb #sc50324 (Santa Cruz Biotechnology), Ki-67 kit/antibody (Dako Inc.); secondary antibodies: goat anti-rabbit IgG HRP-conjugated #7074 (Santa Cruz Biotechnology), anti-rabbit IgG (H+L), $F(ab')_2$ fragment PE conjugate #8885 (Cell Signaling Technology), goat anti-mouse IgG-FITC #sc2010; chemicals: 3-BrPA (Sigma Aldrich), gemcitabine hydrochloride salt (LC Laboratories), succinyl-β-cyclodextrin (β–CD, Sigma Aldrich), D-luciferin potassium salt (Gold Biotechnology); cell culture: RPMI1640 and MEM (Life Technologies), FBS (Thermo Scientific), penicillin/streptomycin (Sigma Aldrich), collagen I Rat Tail (BD Biosciences, #354326), controlled atmosphere chamber (Plas. Labs); invasion assay: Matrigel basement membrane Matrix (BD Biosciences), Matrigel invasion chamber Transwell polycarbonate membrane inserts (Corning); kits: CellTiter-Glo Luminescence Cell Viability Assay Kit, Dual-Luciferase Reporter Assay Kit (Promega), 2D Quant Kit (GE Healthcare), Histostain Plus 3rd Gen ICH Detection Kit (Invitrogen), Diff Quik Stain Kit (Polysciences Inc.); imaging: Zeiss 700 LSM confocal microscope, Olympus IX81 inverted microscope, Eclipse TS100 inverted microscope (Nikon), IVIS200 (Xenogen Corp.)

Microencapsulation of 3-BrPA and nuclear magnetic resonance spectroscopy. Encapsulation of 3-BrPA in β-CD was achieved by portionwise addition of 3-BrPA (166 mg, 1 mmol/L) to a stirring solution of β-CD (1,836 mg in 30 mL DI water). The resulting solution was sonicated for 1 hour at room temperature and then shaken overnight at 25°C, flash frozen, and lyophilized. Encapsulation was confirmed by ^{1}H-NMR experiments performed at 400 MHz on a Bruker Avance spectrometer. The NMR spectra were recorded in 99.9% D_2O and are reported in parts per million downfield relative to tetramethysilane (TMS). Briefly, 10 mmol/L solutions of β-CD alone, 3-BrPA alone, or the complex of 3-BrPA and β-CD were prepared in D_2O containing 1% DSS [3-(trimethylsilyl)-1-propanesulfonic acid, sodium salt; Sigma Aldrich] as an internal standard. Spectra were recorded at 25°C with 32 scans. The ^{1}H-NMR spectra were aligned using signals from the internal standard at 0.64, 1.78, and 2.91 ppm. The spectra of 3-BrPA alone exhibited a singlet for the methylene protons at 3.66 ppm. An upfield shift due to diamagnetic shielding of the methylene protons (0.1 ppm) was observed in the spectrum of the complex confirming encapsulation (Fig. 1A). Further confirmation of microencapsulation was provided by ^{13}C NMR spectroscopy. Samples of β-CD alone, 3-BrPA alone, and the complex were prepared in D_2O (75 mmol/L) containing TMS as an internal standard and recorded at 25°C with 512 scans. The spectra of 3-BrPA alone (Fig. 1B; blue) exhibited 3 signals corresponding to each carbon of its backbone. An upfield shift of each of these signals by >1.5 ppm was observed (Fig. 1B; red). Surface morphology of β-CD, 3-BrPA, and β-CD-3-BrPA was examined by scanning electron microscope (SEM, LEO 1550 FESEM). The samples were dispersed on carbon tabs adhered to aluminum stubs and directly imaged at various magnifications without any

Published OnlineFirst October 17, 2014; DOI: 10.1158/1078-0432.CCR-14-1271

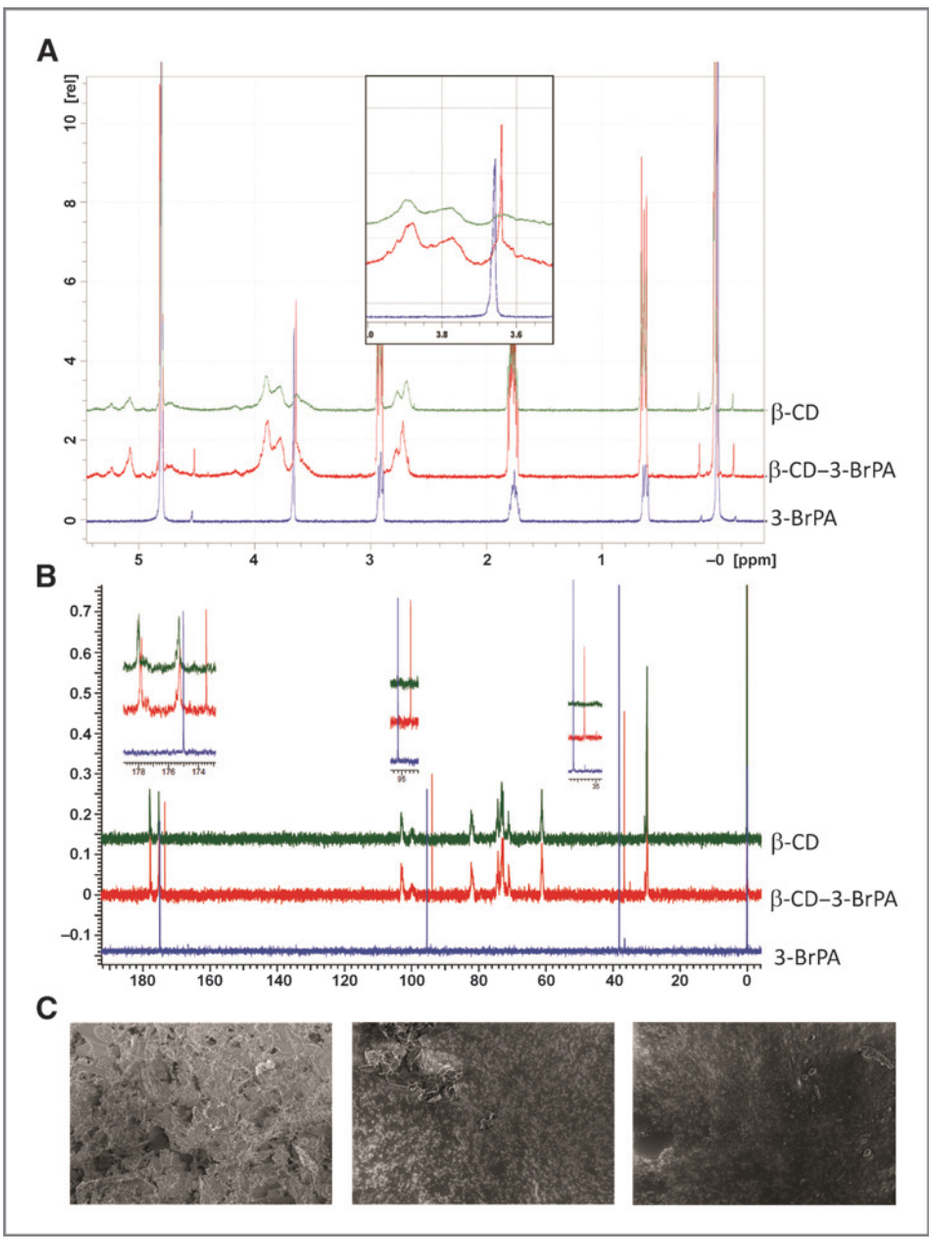

Figure 1. Characterization of microencapsulated 3-BrPA. A, ^{1}H NMR spectra of 3-BrPA (blue), β-CD–3-BrPA complex (red) and β-CD (green) in D_2O. The magnified insert highlights the methylene protons of 3-BrPA and upfield shift of the same methylene protons upon encapsulation of 3-BrPA in β-CD. B, ^{13}C NMR spectra of 3BrPA (blue), β-CD-3-BrPA complex (red), and β-CD (green) in D_2O. The inserts highlight an upfield shift of all 3 carbons of 3-BrPA upon complexation. C, SEM micrographs of 3BrPA (left), β-CD (center), and the β-CD–3-BrPA inclusion complex (right).

coating (Fig. 1C). The surface morphology of both β-CD and 3-BrPA was no longer observed in the complex which showed irregular amorphous particles (Fig. 1C). Further attempts at measuring particle size and dispersity using dynamic light scattering (DLS) and transmission electron microscopy (TEM; Supplementary Fig. S1) failed to yield any result suggesting that β-CD–3-BrPA complexes are completely soluble in water and do not exhibit any particulate nature under our evaluation conditions.

Monolayer cell culture and viability assay. Two human PDAC cell lines, *luc*MiaPaCa-2, stably transfected with the luciferase-aminoglycoside phosphotransferase fusion gene (17), and Suit-2 (kindly provided by Dr. Shinichi Ota, Shiga University of Medical Science, Shiga, Japan) were cultured in RPMI or MEM media, respectively; both supplemented with 10% FBS and 1% penicillin–streptomycin. MiaPaCa-2 was derived from a primary PDAC and Suit-2 was derived from a metastatic PDAC from a different patient (18). Cell lines were authenticated using STR profile analysis (ATCC) and tested for contamination (LookOut qPCR-ProbeKit, Sigma) within 6 months of the last experiment. The effects of different drugs on cell viability were determined by quantifying intracellular ATP levels using a luminescence-based kit (CellTiter-Glo, Promega). The accuracy in *luc*MiaPaCa-2 cells was confirmed using the Dual Reporter Assay Kit (Promega). In brief, 5×10^3 cells were seeded in triplicate and incubated for 72 hours under normoxic or hypoxic (1% O_2 level, balanced

Published OnlineFirst October 17, 2014; DOI: 10.1158/1078-0432.CCR-14-1271

with CO_2 and nitrogen within a controlled atmosphere chamber) conditions. Indicated amounts of free 3-BrPA, 1:1-β-CD–3-BrPA, or β-CD as a control were dissolved in PBS and added to the medium for 24 hours of treatment. For experiments with gemcitabine, cells were incubated for 24 hours before a 72-hour exposure to the drug. Of note, the prolonged time-to-effect of gemcitabine (no effects visible at 24 hours) required a longer incubation with the drug. Thus, the time for preincubation in hypoxia was shorter as compared with 3-BrPA. Cell viability was determined following the manufacturer's protocol.

Three-dimensional organotypic cell culture, imaging, and immunofluorescence. A collagen I-based three-dimensional (3D) organotypic cell culture system was used to mimic an extracellular matrix (ECM)-rich environment and to test the effects of 3-BrPA on tumor invasion (19). Specifically, a collagen solution which initially consisted of 25 μL of 10× DMEM and 217 μL of collagen I (3.83 mg/mL) was prepared on ice. The pH value was adjusted by dropwise addition of sodium hydroxide (Sigma Aldrich) to reach pH = 7.0. The collagen I was then diluted using DMEM F12/GlutaMAX (Life Technologies) to a final concentration of 3 mg/mL. An underlayer was created on the bottom of each well of an uncovered glass-bottom 24-well plate (InVitroScientific) using 15 μL of the collagen solution which was then allowed to polymerize at 37°C for at least 1 hour. The remaining collagen solution was kept on ice for 3 to 5 hours to allow initial polymerization. A total of 65×10^3 *luc*MiaPaCa-2 or 45×10^3 Suit-2 cells were resuspended in a volume of 150 μL collagen solution. By creating a drop with the height of 0.5 cm, the cell suspension was placed on top of the prewarmed underlayer. The collagen–cell suspension was allowed to polymerize for 1 hour at 37°C and subsequently covered with cell culture medium (20).

3D organoids were treated either once or sequentially. For single treatments, embedded cells were incubated for 5 days under normoxic or hypoxic (1% O_2 level within a controlled atmosphere chamber) conditions before treatment. On day 5, medium was replaced by 1:1-β-CD–3-BrPA, 3-BrPA, or β-CD–containing medium and the cells were incubated for 24 hours with the respective concentrations of the drug. For experiments with gemcitabine, cells were allowed to grow for 48 hours before being treated and incubated with the drug for another 72 hours. Initial experiments with gemcitabine did not demonstrate any efficacy after 24 hours (data not shown), and it was thus decided to follow the most commonly reported incubation times of 72 hours. Sequential treatment with 3-BrPA was performed on alternate days for 1 week with each respective dose and evaluated by bright field microscopy (Olympus) at 40× magnification with a 1.3 NA oil objective. A Hamamatsu Photonics C9100-02 EMCCD camera was used to acquire images, which were analyzed with the SlideBook 5.0 program.

Microscopic observations were compared with the quantification of cell viability measured through bioluminescence imaging (BLI). For the latter measurements, the cell culture medium covering the 3D organotypic culture was replaced by 500 μL of a Luciferase substrate (D-Luciferin, potassium salt, Life Technologies, 20 mg/mL) in PBS. After 5 minutes of exposure, the plate was positioned and images were acquired (Xenogen Ivis Imaging System 100). Signal intensity was determined by the photon emission (in counts) and measured within a region of interest (ROI) which enclosed the entire 3D organoids (Living Image Software, PerkinElmer).

The microscopic and BLI findings were verified using immunofluorescence microscopy. 3D organoids were fixed using 4% formaldehyde and cryofixed with optimum cutting temperature (OCT) compound (Tissue Tek) at −80°C. The samples were cut into sections of 100 μm thickness at −20°C. OCT was washed off using PBS, twice for 10 minutes each. Before staining, sections were permeabilized with 0.5% TRIzol-100 in PBS for 30 minutes and washed twice with PBS for 10 minutes each. After blocking with 10% FBS in PBS for 2 hours, samples were incubated with primary antibodies (Alexa Fluor 568 Phalloidin, Invitrogen 1:100; GAPDH Alexa Fluor 488 Conjugate Cell Signaling Technology 1:800, cleaved caspase-3 Cell Signaling Technology 1:500, HIF-1α 1:50) for 1 hour at room temperature under light protection. For nonconjugated primary antibodies, additional incubation with a phycoerythrin- or FITC-conjugated secondary antibody for 1 hour at room temperature was used. This was followed by two washes with PBS for 10 minutes each. DAPI was used as a counter stain at a concentration of 300 ng/mL and added to the specimen simultaneously with the conjugated antibodies. Confocal fluorescence microscopy was performed at 40× magnification with 1.4 NA oil objective and 63× with 1.4 NA oil objective, and images analyzed with Zen2012 software. Excitation and emission wavelengths were those recommended by the conjugate manufacturers.

Matrigel invasion assay, zymography, and immunoblotting. The ability of 3-BrPA to inhibit tumor invasion was studied using Matrigel invasion assay and gelatin zymography (21). For the Matrigel invasion assays, a coating buffer containing 0.01 mol/L Tris and 0.7% sodium chloride was prepared and used to dilute the Matrigel basement membrane to 300 μg/mL. Subsequently, Boyden chambers (Transwell, Corning; 6.5 mm diameter, 8 μm pore size) were coated with 100 μL Matrigel solution and stored at 37°C for 2 hours to allow gelatination. Approximately 7.5×10^4 cells were resuspended in 500 μL FBS-free medium and plated into the top chamber of the insert, which was then placed into a 24-well plate containing 750 μL of FBS-containing medium. After overnight incubation at 37°C, various amounts of 3-BrPA were added to the top chamber. Forty-eight hours later, noninvasive cells were removed from the top of the Matrigel with a cotton swab. Invaded cells adherent to the bottom side of the permeable insert were fixed and stained with the Diff Quik Stain Kit (Polysciences Inc.). Light microscopy was performed at 4×, 10×, and 20× magnification. Invasion of cells was quantified by measuring the area of stained cells after treatment and compared with untreated samples at 10× magnification.

Published OnlineFirst October 17, 2014; DOI: 10.1158/1078-0432.CCR-14-1271

Zymography assays were performed to determine the activity of secreted MMP-9. Accordingly, 4×10^6 Suit-2 cells and 2.5×10^6 *luc*MiaPaCa-2 cells were seeded in 75 cm^2 flasks and incubated overnight at 37°C under normoxic conditions. The following day, fresh FBS-free medium containing different concentrations of 3-BrPA was added and cells were incubated for an additional 24 hours. Subsequently, supernatants were collected, filtered, and the final protein concentrations were determined using the 2D Quant Kit (GE Healthcare). Each sample was loaded on two 10% gelatin zymography gels (Novex, Invitrogen). Following electrophoresis, proteins in one of the two gels were renatured and enzymatic digestion was allowed to proceed overnight at 37°C in a developing buffer. The gel was stained with 4 parts 0.1% Coomassie brilliant blue in 1 part 100% methanol for 24 hours and washed with DI water until digested areas were detectable as white bands. Western blot analysis was performed with the duplicate gel. Proteins were blotted onto a PVDF membrane and blocked using 5% skimmed milk in 1× TBS and 0.1% Tween in DI (TBST). Primary anti-MMP antibody (Cell Signaling Technology) was used in a 1:1,000 dilution and incubated at 4°C overnight, followed by an HRP-conjugated secondary antibody (Santa Cruz Biotechnology) incubation for 1 hour at room temperature. The HRP provided an electrochemiluminescence signal (ECL Kit, GE Healthcare) which was analyzed with ImageJ 1.46r software (Wayne Rasband, NIH, Bethesda, MD) and used to quantify signal intensity by comparing line integrals.

In vivo studies

Orthotopic animal xenografts. Male athymic nude mice (body weight, 20–25 g; 4 weeks old; Crl:NU (NCr)-Foxn1^{nu}; Charles River Laboratory) were used in accordance with institutional guidelines under approved Animal Care and Use Committee protocols. Mice were maintained in laminar flow rooms at constant temperature and humidity, with food and water given *ad libitum*. Orthotopic xenograft tumors were generated by implantation of 1.5×10^6 *luc*MiaPaCa-2, suspended in 50 μL PBS, into the tail of the pancreas. To accomplish this, mice were placed into an anesthesia induction chamber (oxygen flow rate, 1 L/minute; isoflurane concentration of 3%–4%). Upon loss of the righting reflex, animals were placed on the surgical procedure surface, where a nose cone was used to maintain anesthesia (oxygen flow, 0.8 L/minute; isoflurane concentration, 1.5%–2%). A small, left abdominal flank incision was made, and the pancreas was exteriorized before injecting the cell solution with a 30 G Hamilton syringe. A successful subcapsular intrapancreatic injection was identified by the appearance of a fluid bleb without intraperitoneal leakage. The abdominal cavity was closed with nonabsorbable suture material (22).

BLI and ultrasound imaging. Tumor viability was confirmed via *in vivo* bioluminescence imaging (BLI) on day 7 after the surgical implantation. Anesthetized tumor-bearing mice were injected intraperitoneally with D-luciferin, 150 mg/kg, and optically imaged 5 minutes later using the IVIS 200 system (Xenogen). The pseudocolor image representing the spatial distribution of photons was overlaid on a previously acquired grayscale photographic image. A ROI was created to include the optical tumor image. Signal intensity was quantified within the ROI in photons/second/squared centimeter/steradian (p/s/cm^2/Sr) after a 10-second exposure using Living Image software (Xenogen). In addition, orthotopic growth of the tumors was confirmed before treatment using small-animal ultrasound imaging (USI). In brief, anesthetized mice were subjected to examination using the VEVO2100 (Visual Sonics Inc., kindly provided by Dr. Harry C. Dietz, Johns Hopkins University School of Medicine) by applying a MS-550D MicroScan transducer probe with 40 MHz (broadband with 22–55 MHz). Tumor localization was confirmed using the cranial tip of the left kidney and the caudal tip of the spleen as anatomic landmarks (13, 17).

Treatment regimen and imaging follow-up. Animals with tumors, as confirmed by both BLI and USI, were randomized into four groups: group 1 ($n = 21$ animals) received daily intraperitoneal injections of the β-CD–3-BrPA complex (5 mg/kg 3-BrPA in 53 mg/kg β-CD, dissolved in 500 μL saline), group 2 ($n = 7$ animals) received intraperitoneal injections of gemcitabine (150 mg/kg dissolved in 200 μL saline, three injections/week, as commonly reported in literature; refs. 23, 24), group 3 ($n = 7$) received daily intraperitoneal injections of β-CD alone (53 mg/kg β-CD, dissolved in 500 μL saline), and group 4 ($n = 7$ animals) received daily intraperitoneal injections of 3-BrPA alone (5 mg/kg dissolved in 500 μL saline). All animals were treated without interruptions for a period of 4 weeks. Follow-up BLI was acquired on day 7, 14, 21, and 28 after the first injection. Animals were sacrificed on day 28 after the last imaging session or when moribund.

Immunohistochemistry. Healthy organ tissue and tumors were obtained, fixed with a 4% formaldehyde solution for a period of at least 72 hours, and embedded in paraffin. Hematoxylin and eosin (H&E) staining of the slides was performed according to standard protocols (25). Tumor sections (18 μm thick) were stained for the following targets: GAPDH, MCT-1, cleaved caspase-3, and Ki-67 using the Histostain Plus 3rd Gen IHC Detection Kit (Invitrogen) as well as the Ki-67 kit (Dako Inc.). Specifically, specimens were deparaffinized using xylene and rehydrated using a descending ethanol dilution series. After washing with deionized water, samples were permeabilized in boiling retrieval solution containing citrate for 40 minutes at 95°C. Specimens were cooled to room temperature and incubated with 2 drops (~100 μL total) of peroxidase quenching solution for 5 minutes and blocked for 20 minutes. Incubation with primary antibodies (GAPDH, 1:500; MCT-1, 1:250; Ki-67 and HIF-1α; 1:50, cleaved caspase-3, 1:1500; in PBS) occurred at room temperature in a moist chamber for 60 minutes. Biotinylated secondary antibody and streptavidin–peroxidase conjugate were added to the samples in sequence for 10 minutes each. Twenty-six microliters of 3,3′-diaminobenzidine (DAB) chromogen were mixed well with 1 mL of DAB subtrate

Published OnlineFirst October 17, 2014; DOI: 10.1158/1078-0432.CCR-14-1271

buffer and 100 μL were added to each specimen for 5 minutes. Hematoxylin was used as a counterstain. Incubation steps were followed by washing once with distilled water and twice with PBS for 2 minutes each. All slides were scanned and digitized at a 20× magnification using a High-Resolution Aperio Scanner System (Vista). The digitized slides were then assessed using ImageScope software. For the Ki-67–stained tissue sections, the Ki-67 proliferation index [formula: Index (%) = number of positive cells/total cell number × 100] was calculated as described elsewhere (13).

Statistical analysis

All experiments were performed independently and repeated at least three times. Data from the experiments were summarized with means ± SEM. Statistical comparisons of data sets were evaluated by the student *t* test as well as the one-way ANOVA test. Reported BLI signal intensities were normalized among the animals and reported as multiples based on the baseline value.

Results

In vitro

Effects of β-CD–3-BrPA on 2D and 3D cell cultured pancreatic cancer cells. Upon NMR spectroscopic confirmation of the complexation between 3-BrPA and β-CD (Fig. 1A and B), the microencapsulated formulation of the drug was used for further experiments. The measurements of particle size and dispersity using DLS and TEM did not result in a measureable result due to complete solubility of the complex in water. To assess the ability of microencapsulated 3-BrPA (β-CD-3-BrPA) to achieve dose-dependent ATP depletion and cell death, two human pancreatic cancer cell lines were employed. The dose-dependent effects of β-CD–3-BrPA were compared with free 3-BrPA as well as with gemcitabine, and β-CD was used as a control. As hypoxia is often associated with chemoresistance in PDACs, hypoxic exposure was added to the experimental design (26–28). We found that β-CD–3-BrPA and free 3-BrPA demonstrated similar cytotoxicity profiles under normoxic (50–75 μmol/L) as well as hypoxic (12.5–25 μmol/L) conditions, but, interestingly, both PDAC cell lines were more sensitive to the drugs when hypoxic (Fig. 2). Cell lines treated with β-CD alone were perfectly viable throughout the experiment, even when exposed to very high concentrations. Similar results were observed in Suit-2 cells but with less pronounced differences between normoxic and hypoxic conditions (Fig. 2). While assessing the efficacy of gemcitabine, IC_{50} in MiaPaCa-2 and Suit-2 cells was barely achieved under normoxic conditions (0.1 μmol/L), no concentration achieved a complete kill, and hypoxia seemed to increase the resistance towards the drug.

To test the efficacy of β-CD–3-BrPA in an ECM-rich environment, *luc*MiaPaCa-2 cells were cultured in a 3D collagen 1 matrix and treated with a single dose of either β-CD–3-BrPA, free 3-BrPA or β-CD (as a control; Fig. 2, bottom). BLI quantification showed that both drug formulations had equivalent potencies in normoxic conditions (IC_{50}, 25–50 μmol/L; Fig. 2, bottom, blue lines). Under hypoxic conditions, MiaPaCa-2 cells were slightly more sensitive to free 3-BrPA than to β-CD–3-BrPA (Fig. 2, bottom, red line). As for gemcitabine, significant differences in efficacy were observed between normoxic and hypoxic conditions under which the drug failed to achieve any meaningful effect even at molar concentrations (Fig. 2, bottom). The cells cultured in 3D were treated sequentially with the drugs, as described in Materials and Methods. Morphologic, BLI, and immunofluorescence-based analysis confirmed the ability of 3-BrPA to penetrate an ECM-rich matrix and to inhibit cell proliferation as well as to induce apoptosis (Supplementary Fig. S2). Untreated MiaPaCa-2 cells proliferated and formed "grape"-like structures within the collagen 1 matrix, whereas Suit-2 cells demonstrated a more invasive morphology with cellular protrusions visible after 6 days of growth (Supplementary Fig. S2). When treated with 3-BrPA, proliferation in both cell lines was inhibited with a morphologically visible reduction of cell protrusions in Suit-2 cells (Supplementary Fig. S2). In addition, immunofluorescence imaging confirmed a dose-dependent induction of apoptosis by 3-BrPA.

Targeting metabolism reduces the invasive potential of pancreatic cancer cells. The ability of 3-BrPA to inhibit the invasiveness of pancreatic cancer cells at sublethal drug concentrations was tested using a Matrigel invasion assay. As shown in Fig. 3A and B, both the MiaPaCa-2 and Suit-2 cells showed a reduction in invasion at drug concentrations as low as 12.5 μmol/L. In addition, the effect of sublethal doses of 3-BrPA on the secretion of the MMP-9, a well-described marker for the invasive potential of pancreatic cancer cells, was tested using gelatin zymography and immunoblotting (29–31). Accordingly, a marked reduction in the secretion of MMP-9 was detected in both cell lines. This effect was observed beginning with a 3-BrPA concentration of 6.25 μmol/L (a dose that did not induce apoptosis or reduce cell viability) and an earlier onset in the more metastatic Suit-2 cell line (Fig. 3C and D).

***Systemic delivery of β-CD–3-BrPA achieves strong anticancer effects* in vivo.** The anticancer efficacy of systemically delivered β-CD–3-BrPA was tested on an orthotopic xenograft model of human pancreatic cancer in athymic nude mice. Before choosing the therapeutic dose for more detailed studies, comparative dose escalation studies in non–tumor-bearing animals were performed for both β-CD–3-BrPA and free 3-BrPA. Accordingly, 20 mg/kg of β-CD–3-BrPA and 10 mg/kg free 3-BrPA were identified as the median lethal doses (LD_{50}) after a single injection and 5 mg/kg β-CD-3-BrPA was identified as a safe dose that did not cause any toxicity when given systemically and daily over the course of 7 days. A total of 42 animals with orthotopically implanted and BLI- and USI-confirmed MiaPaCa-2 tumors were then randomized to receive intraperitoneal injections of β-CD-3-BrPA ($n = 21$), gemcitabine ($n = 7$) or β-CD ($n = 7$). An

Published OnlineFirst October 17, 2014; DOI: 10.1158/1078-0432.CCR-14-1271

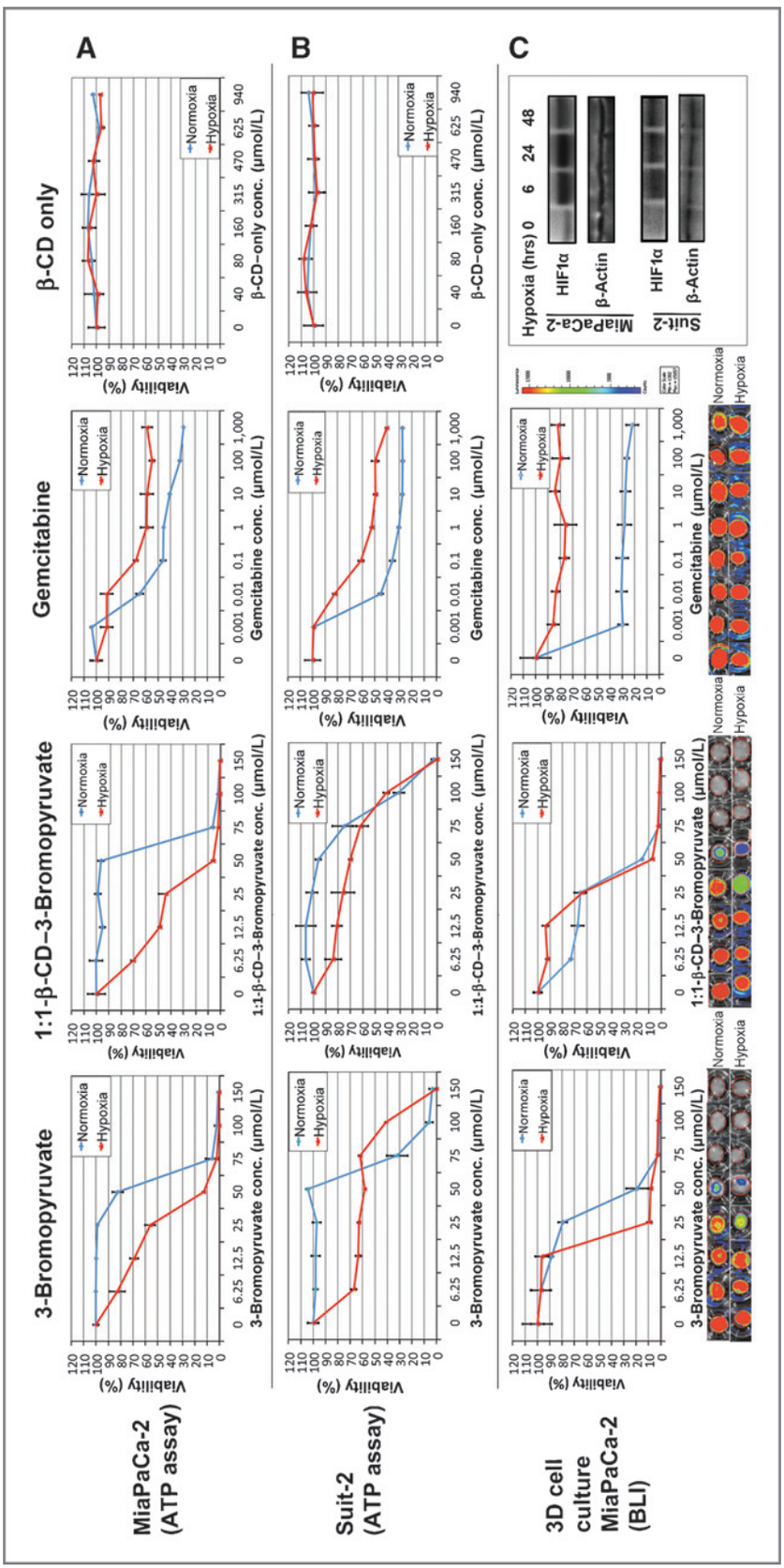

Figure 2. Kill curves in 2D and 3D organotypic cell culture. This figure illustrates the luminescence-based cell viability of MiaPaCa-2 (A, top row) and Suit-2 (B, middle row) cells after various treatments. Cells were incubated under normoxic or hypoxic conditions for 72 hours before exposure to 3-BrPA, 1:1-β-CD–3-BrPA or β-CD for 24 hours. Cells were incubated for 24 hours before being treated with gemcitabine for 72 hours. For the 3D organotypic cell cultures (C, bottom row), *luc*MiaPaCa-2 cells were incubated under normoxic or hypoxic conditions for a total of 6 days; single treatments with 3-BrPA or β-CD–3-BrPA were performed on day 5 for 24 hours. Exposure to gemcitabine was initiated on day 3 for 72 hours (due to the longer time-to-effect for this drug). Bioluminescence imaging was performed on day 6 to evaluate drug penetration and effects on cell viability. The bottom right box contains the immune-blots for HIF-1α to confirm that hypoxia was present.

Published OnlineFirst October 17, 2014; DOI: 10.1158/1078-0432.CCR-14-1271

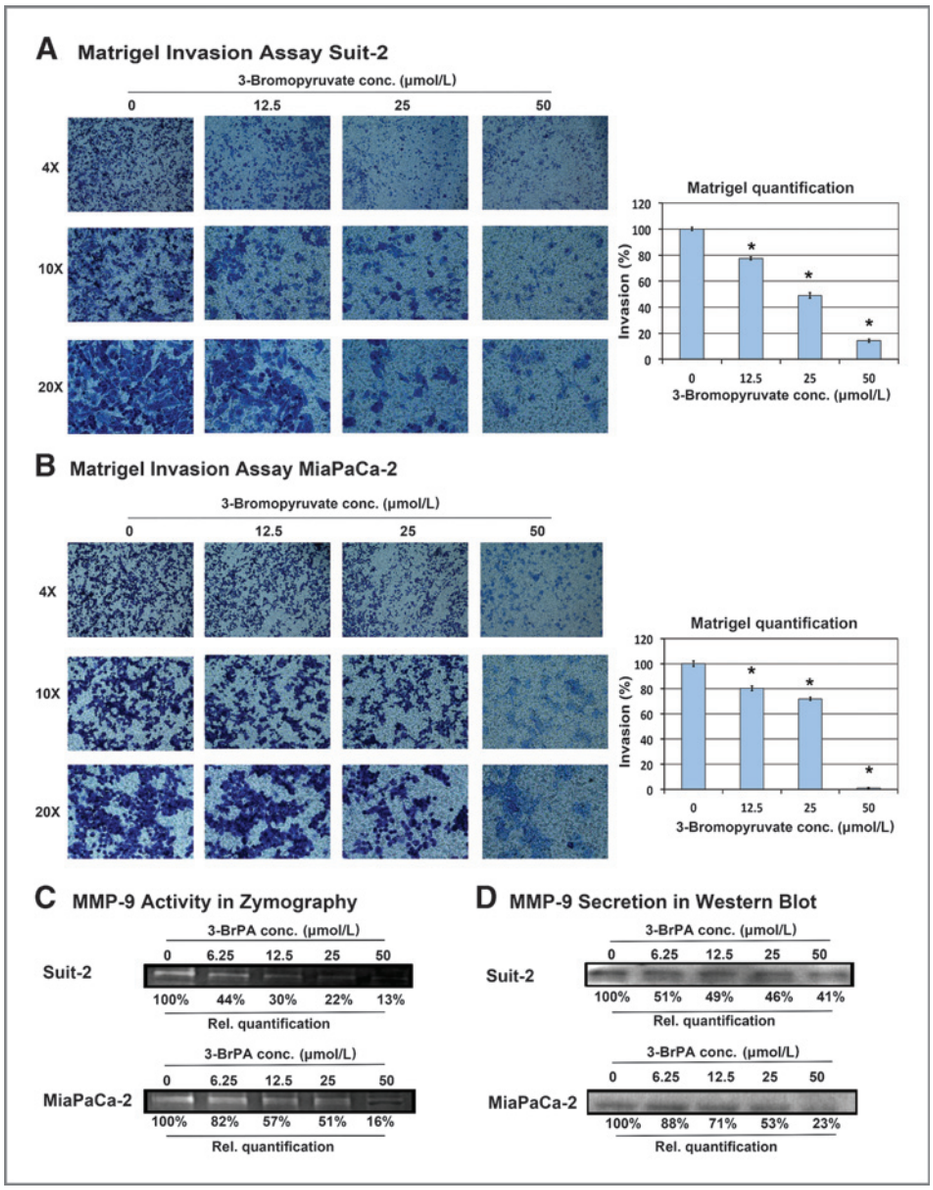

Figure 3. Effects of 3-BrPA on cell invasiveness. MiaPaCa-2 (A) and Suit-2 (B) cells were plated into a Boyden invasion chamber. Incubation overnight was followed by treatment with 3-BrPA for 48 hours (MiaPaCa-2) or 72 hours (Suit-2). Invaded cells on the bottom side of the membrane of the invasion insert were stained using a Giemsa-like staining. Images show invaded cells at 4×, 10×, and 20× magnification. Relative quantification of invasion was calculated by measuring the area of stained cells in the entire field of view at 10×. MMP-9 activity and secretion were determined in the concentrated supernatant of MiaPaCa-2 and Suit-2 cells by zymography (C) and Western blot analysis (D). *, indicates statistically significant differences ($P < 0.05$).

additional group of animals with orthotopic implants ($n = 7$) was treated with free 3-BrPA. Daily intraperitoneal injections of free 3-BrPA (5 mg/kg in 500 μL saline) elicited high treatment-related toxicity and 3 of 7 (43%) animals died before the acquisition of the first follow-up BLI (Supplementary Fig. S3A). At the end of the experiment (day 28), only 2 of 7 animals (28%) treated with the free drug survived (Supplementary Fig. S3A). No such toxicity was observed in the remaining groups. At the conclusion of the experiment, all animals were subjected to necropsies and organs (brain, heart, lungs, bowel, liver, and kidneys) were harvested for the analysis of potential organ damage. No organ toxicities or tissue damage was observed in animals treated with β-CD–3-BrPA (Supplementary Fig. S3B).

Daily intraperitoneal injections of β-CD–3-BrPA (5 mg/kg in 500 μL saline) demonstrated strong anticancer effects with early effects visible on day 14 after the first injection (Fig. 4B). After 4 weeks of treatment, a comparison of BLI signal intensity between the groups was performed. Animals treated with the β-CD control demonstrated a 140-fold signal increase over baseline. A moderate deceleration of tumor growth was observed in gemcitabine-treated animals with a 60-fold signal increase over time. Most importantly, animals treated with β-CD–3-BrPA showed minimal or no progression of the signal (Fig. 4). After achieving this endpoint, animals were sacrificed and tumors were harvested for further analysis. The analysis of tumor pathology demonstrated vast tumor destruction with central areas of colliquative necrosis in

Published OnlineFirst October 17, 2014; DOI: 10.1158/1078-0432.CCR-14-1271

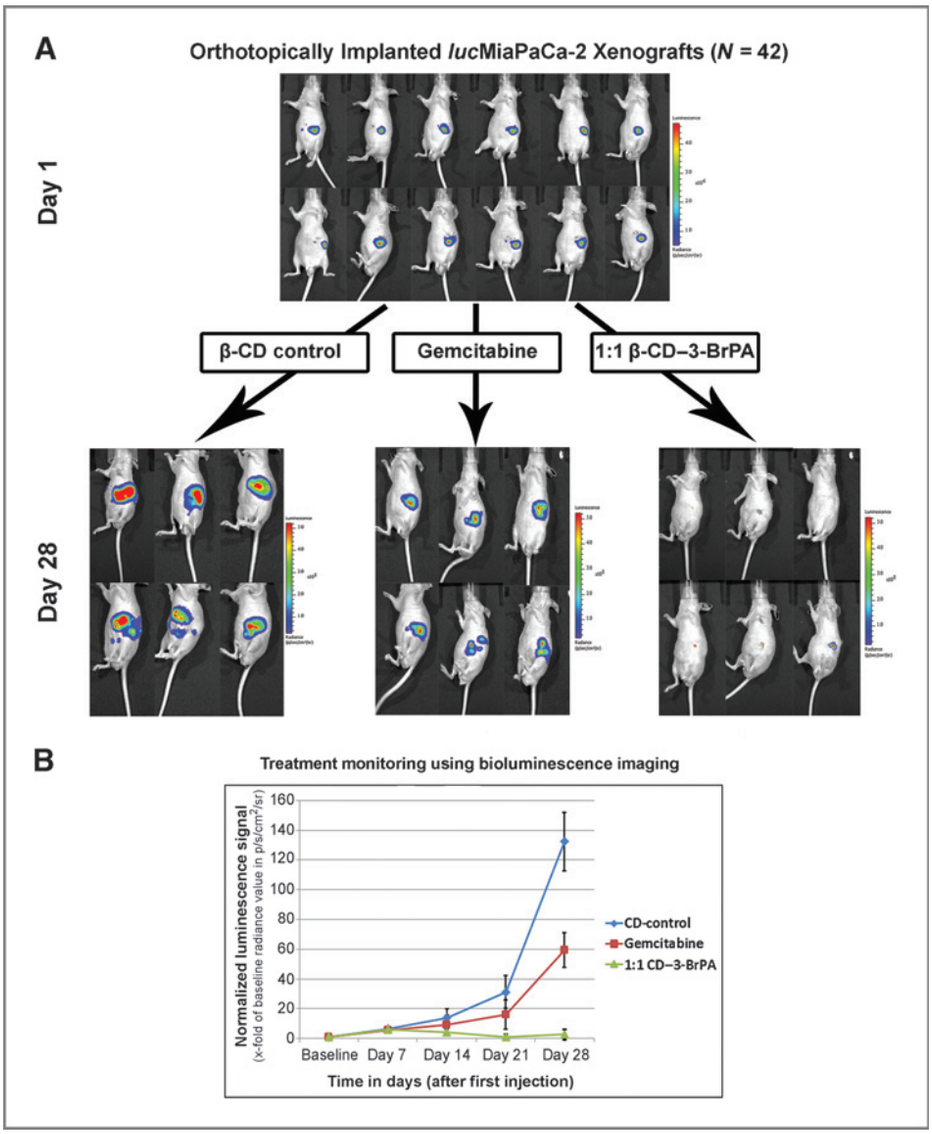

Figure 4. *In vivo* efficacy of β-CD–3-BrPA. A total of 42 male nude mice were orthotopically implanted with a total of 1.5×10^6 *luc*MiaPaCa-2 cells. After one week of xenograft growth, tumors were confirmed using bioluminescence imaging (BLI). A representative number of animals are shown in (A). Animals were randomized to receive β-CD–3-BrPA ($n = 21$), free 3-BrPA ($n = 7$), gemcitabine ($n = 7$), and β-CD ($n = 7$). Animals were imaged once per week over the course of 28 days. The overall progress of the signal is demonstrated in B. Animals treated with free 3-BrPA showed high treatment-related toxicity and did not survive in statistically relevant numbers to be included in the final image analysis.

animals treated with β-CD–3-BrPA (Fig. 5). Tumor regions with intact cell junctions demonstrated a high expression of cleaved caspase-3, indicating fulminant tumor apoptosis. Animals treated with β-CD–3-BrPA demonstrated a significant reduction in proliferation as assessed with Ki67 immunohistochemistry, 3-fold more prominent than observed with gemcitabine treatment (Fig. 5). In addition, animals treated with β-CD–3-BrPA demonstrated lower expression levels of MCT1 and GAPDH within the treated tumors as compared with the β-CD or gemcitabine groups.

Discussion

The main finding of this study is that systemically delivered β-CD–3-BrPA achieved strong antitumoral effects *in vivo* while causing much less toxicity in therapeutic doses when compared with the free drug. Furthermore, microencapsulation of 3-BrPA did not alter the efficacy of the drug against pancreatic cancer cells *in vitro*, which was demonstrated using two dimensional (2D) as well as ECM-rich 3D cell cultures, both under normoxic and hypoxic conditions. The ability of 3-BrPA to inhibit the secretion of MMP-9 and to reduce the invasiveness of pancreatic cancer cells in sublethal doses further supports the anticancer potential of this drug.

Selectively targeting tumor metabolism has long been considered as a desirable therapeutic option but has not yet been translated into clinical practice. The primary limitation in reaching the milestone of systemic deliverability with 3-BrPA is the reported toxicity due to its alkylating properties (10, 15, 32). As a result, local image-guided delivery of the drug has been explored as an alternative therapeutic option; however, the practical use of these approaches is limited to treating localized

Published OnlineFirst October 17, 2014; DOI: 10.1158/1078-0432.CCR-14-1271

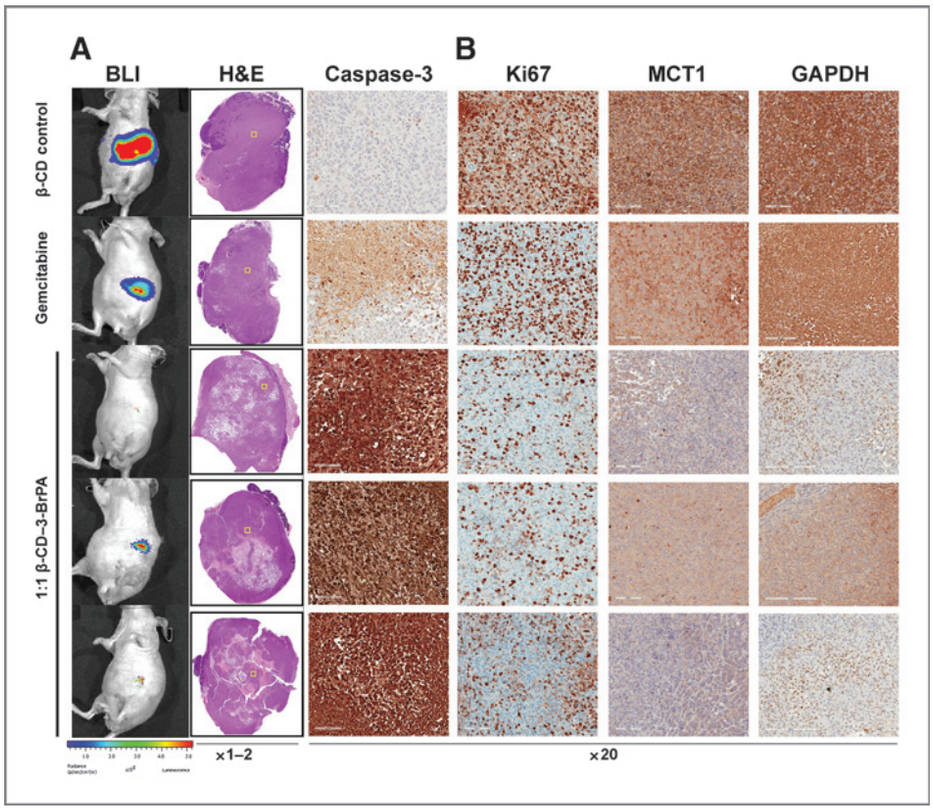

Figure 5. *Ex vivo* pathologic and immunohistochemical tumor analysis. The H&E staining of tumors treated with β-CD, gemcitabine or β-CD–3-BrPA (3 representative tumors are shown here under A) demonstrated the treatment effects of β-CD–3-BrPA. The yellow squares within the H&E-stained whole-tumor overviews indicate the areas magnified for further analysis of the antitumoral effects of the drugs, which was confirmed by the staining for cleaved caspase-3 and Ki-67 (B). In addition, the marked reduction of GAPDH as the primary target of 3-BrPA as well as MCT-1 as the specific transporter becomes apparent (B). Of note, only areas that did not show complete/liquefied necrosis were selected for analysis in higher magnification.

disease (13, 14). Here, we clearly demonstrate that the drug, when appropriately formulated for systemic delivery, was extremely effective in two experimental systems, thereby expanding the use of this compound, in theory, to virtually any cancer. Our results with the free drug are not dissimilar to those of the only other study where the drug was used systemically to treat solid tumors. In that study, free 3-BrPA failed to elicit any meaningful tumor response at slightly lower doses as used in our experiments (16, 33). We saw some efficacy at these doses, but excessive and prohibitive toxicity, with treatment-related deaths in most animals, was the predominant result. It is possible that in the microencapsulated formulation, 3-BrPA, is more bioavailable for uptake into tumor cells and less available to the normal cells that apparently mediate its toxicity (12, 34, 35). The emerging role of cyclodextrins as versatile platforms for drug delivery has been demonstrated for many drugs with unfavorable pharmacokinetics. Future studies should further characterize the pharmacokinetic and structural properties of the β-CD–3-BrPA (35).

A characteristic feature of pancreatic tumor tissue is the excessive accumulation of dense ECM which limits oxygen diffusion and creates a highly hypoxic, ill perfused tumor microenvironment known for its profound chemoresistance, and increased invasiveness (7, 31). Published studies confirmed that more than 30% of pancreatic tumor cells are located in poorly vascularized, hypoxic tumor compartments, thereby escaping the effects of conventional chemotherapy and ionizing radiation (36). Conflicting data have been reported for the oxygen dependency of 3-BrPA in cancer cells (37, 38). However, there is significant evidence in support of our finding that 3-BrPA is effective even under hypoxic conditions (39). Specifically, recent studies have established the link between hypoxia and the expression of MCT-1, which was shown to be overexpressed in hypoxic cells, thus providing a plausible explanation for the increased sensitivity of hypoxic tumor tissue towards 3-BrPA (40).

The 3D cell culture model used in our study is composed of a matrix which mimics the collagen 1-rich ECM as seen in human *ex vivo* samples (41). While the benefits of such *in vitro* models for the purpose of drug testing are increasingly recognized, mimicking these conditions *in vivo* represents a greater challenge (42). When designing this study, different animal models were considered. On the one hand, using a widely recognized orthotopic xenograft model has important advantages such as reproducibility, predictable tumor growth dynamics as well as allowing for genomic modification of tumor cells to express specific and imageable reporter genes (22). On the other hand, the degree to which these models reflect the tumor microenvironment in human lesions remains unknown. Although several well-defined mouse tumor models are able to mimic the ECM component and tumor hypoxia more faithfully, these models are less suitable for the purpose of standardized drug testing (36).

Published OnlineFirst October 17, 2014; DOI: 10.1158/1078-0432.CCR-14-1271

An additional unexpected result was observed in the immunohistochemical analysis of treated tumor tissues: next to the anticipated and previously reported depletion of GAPDH as the molecular target of 3-BrPA, the amount of MCT-1 as the specific transporter for 3-BrPA was significantly reduced in treated samples (43). Before this observation, there was no evidence that MCT-1 was a potential target of 3-BrPA. Yet, this lactate transporter has been repeatedly identified as a suitable molecular target for cancer therapy and its relationship to 3-BrPA is worthy of further exploration (44–46).

In summary, the microencapsulation of 3-BrPA is a promising step towards finally achieving the goal of systemically deliverable antiglycolytic tumor therapy. The strong anticancer effects of β-CD–3-BrPA and the favorable toxicity profile pave the way toward clinical trials in patients with pancreatic cancer and potentially other malignancies.

Disclosure of Potential Conflicts of Interest

B. Vogelstein has ownership interest (including patents) in PGDx and PapGene, Inc., is a consultant/advisory board member for Symex-Inostics, and has provided expert testimony for licensed Inventions through Johns Hopkins University. J.F. Geschwind is the CEO and Founder of PreScience Labs; reports receiving a commercial research grant from Philips; and is a consultant/advisory board member for Biocompatibles BTG, Guerbert, Nordion, and Philips. No potential conflicts of interest were disclosed by the other authors.

Authors' Contributions

Conception and design: J. Chapiro, S. Sur, L. Jeanette Savic, S. Ganapathy-Kanniappan, R. Duran, A.J. Ewald, B. Vogelstein, J.-F. Geschwind

Development of methodology: J. Chapiro, S. Sur, L. Jeanette Savic, R. Duran, S. Chettiar-Thiruganasambandam, P. Tran, A.J. Ewald, J.-F. Geschwind

Acquisition of data (provided animals, acquired and managed patients, provided facilities, etc.): J. Chapiro, S. Sur, L. Jeanette Savic, J. Reyes, R. Duran, S. Chettiar-Thiruganasambandam, W. Luo, A.J. Ewald, J.-F. Geschwind

Analysis and interpretation of data (e.g., statistical analysis, biostatistics, computational analysis): J. Chapiro, L. Jeanette Savic, S. Ganapathy-Kanniappan, R. Duran, S. Chettiar-Thiruganasambandam, M. Lin, A.J. Ewald, B. Vogelstein, J.-F. Geschwind

Writing, review, and/or revision of the manuscript: J. Chapiro, S. Sur, L. Jeanette Savic, S. Ganapathy-Kanniappan, R. Duran, M. Lin, W. Luo, P. Tran, J.M. Herman, A.J. Ewald, B. Vogelstein, J.-F. Geschwind

Administrative, technical, or material support (i.e., reporting or organizing data, constructing databases): J. Chapiro, L. Jeanette Savic, S. Ganapathy-Kanniappan, R. Duran, M. Lin, P. Tran

Study supervision: J. Chapiro, L. Jeanette Savic, R. Duran, J.-F. Geschwind

Other (veterinary support for animals in the study): C.R. Moats

Other (provided advice on study design and data interpretation): G.L. Semenza

Acknowledgments

The authors thank Kim-Vy Nguyen-Ngoc, Dr. Laura Wood, MD, PhD, Djahida Bedja, Swathi Karthikeyan, and Eliahu Miller for their technical support in designing and performing the experiments.

Grant Support

This study was funded by NIH/NCI R01 CA160771, P30 CA006973, NCRR UL1 RR 025005 and DODCDMRP, L. Jeanette Savic, S. Ganapathy-Kanniappan, R. Duran, M. Lin, P. Tran W81XWH-11-1-0343 (to J.-F. Geschwind and S. Ganapathy-Kanniappan), the Rolf W. Günther Foundation for Radiological Science (to J. Chapiro and L. Jeanette Savic), RSG-12-141-01-CSM from the American Cancer Society (to A.J. Ewald), NIH grant K99-CA168746 (to W. Luo and G.L. Semenza), NIH grant R01CA166348 (to P. Tran), the Virginia and D.K. Ludwig Fund for Cancer Research, and the Lustgarten Foundation (to B. Vogelstein).

The costs of publication of this article were defrayed in part by the payment of page charges. This article must therefore be hereby marked *advertisement* in accordance with 18 U.S.C. Section 1734 solely to indicate this fact.

Received May 16, 2014; revised September 5, 2014; accepted September 11, 2014; published OnlineFirst October 17, 2014.

References

1. Siegel R, Ma J, Zou Z, Jemal A. Cancer statistics, 2014. CA Cancer J Clin 2014;64:9–29.
2. Hidalgo M. Pancreatic cancer. N Engl J Med 2010;362:1605–17.
3. Hanahan D, Weinberg RA. Hallmarks of cancer: the next generation. Cell 2011;144:646–74.
4. Chu GC, Kimmelman AC, Hezel AF, DePinho RA. Stromal biology of pancreatic cancer. J Cell Biochem 2007;101:887–907.
5. Mahadevan D, Von Hoff DD. Tumor-stroma interactions in pancreatic ductal adenocarcinoma. Mol Cancer Ther 2007;6:1186–97.
6. Muerkoster S, Wegehenkel K, Arlt A, Witt M, Sipos B, Kruse ML, et al. Tumor stroma interactions induce chemoresistance in pancreatic ductal carcinoma cells involving increased secretion and paracrine effects of nitric oxide and interleukin-1beta. Cancer Res 2004;64:1331–7.
7. Yokoi K, Fidler IJ. Hypoxia increases resistance of human pancreatic cancer cells to apoptosis induced by gemcitabine. Clin Cancer Res 2004;10:2299–306.
8. Guillaumond F, Iovanna JL, Vasseur S. Pancreatic tumor cell metabolism: focus on glycolysis and its connected metabolic pathways. Arch Biochem Biophys 2014;545:69–73.
9. Warburg O, Wind F, Negelein E. The metabolism of tumors in the body. J Gen Physiol 1927;8:519–30.
10. Ganapathy-Kanniappan S, Geschwind JF. Tumor glycolysis as a target for cancer therapy: progress and prospects. Mol Cancer 2013;12:152.
11. Ganapathy-Kanniappan S, Geschwind JF, Kunjithapatham R, Buijs M, Vossen JA, Tchernyshyov I, et al. Glyceraldehyde-3-phosphate dehydrogenase (GAPDH) is pyruvylated during 3-bromopyruvate mediated cancer cell death. Anticancer Res 2009;29:4909–18.
12. Birsoy K, Wang T, Possemato R, Yilmaz OH, Koch CE, Chen WW, et al. MCT1-mediated transport of a toxic molecule is an effective strategy for targeting glycolytic tumors. Nat Genet 2013;45:104–8.
13. Ota S, Geschwind JF, Buijs M, Wijlemans JW, Kwak BK, Ganapathy-Kanniappan S. Ultrasound-guided direct delivery of 3-bromopyruvate blocks tumor progression in an orthotopic mouse model of human pancreatic cancer. Target Oncol 2013;8:145–51.
14. Geschwind JF, Ko YH, Torbenson MS, Magee C, Pedersen PL. Novel therapy for liver cancer: direct intraarterial injection of a potent inhibitor of ATP production. Cancer Res 2002;62:3909–13.
15. Chang JM, Chung JW, Jae HJ, Eh H, Son KR, Lee KC, et al. Local toxicity of hepatic arterial infusion of hexokinase II inhibitor, 3-bromopyruvate: *In vivo* investigation in normal rabbit model. Acad Radiol 2007;14:85–92.
16. Cao X, Bloomston M, Zhang T, Frankel WL, Jia G, Wang B, et al. Synergistic antipancreatic tumor effect by simultaneously targeting hypoxic cancer cells with HSP90 inhibitor and glycolysis inhibitor. Clin Cancer Res 2008;14:1831–9.
17. Tuli R, Surmak A, Reyes J, Hacker-Prietz A, Armour M, Leubner A, et al. Development of a novel preclinical pancreatic cancer research model: bioluminescence image-guided focal irradiation and tumor monitoring of orthotopic xenografts. Transl Oncol 2012;5:77–84.
18. Kitamura N, Iwamura T, Taniguchi S, Yamanari H, Kawano MA, Hollingsworth K, et al. High collagenolytic activity in spontaneously highly metastatic variants derived from a human pancreatic

Published OnlineFirst October 17, 2014; DOI: 10.1158/1078-0432.CCR-14-1271

cancer cell line (SUIT-2) in nude mice. Clin Exp Metastasis 2000; 18:561–71.
19. Cheung KJ, Gabrielson E, Werb Z, Ewald AJ. Collective invasion in breast cancer requires a conserved basal epithelial program. Cell 2013;155:1639–51.
20. Nguyen-Ngoc KV, Ewald AJ. Mammary ductal elongation and myoepithelial migration are regulated by the composition of the extracellular matrix. J Microsc 2013;251:212–23.
21. Kupai K, Szucs G, Cseh S, Hajdu I, Csonka C, Csont T, et al. Matrix metalloproteinase activity assays: importance of zymography. J Pharmacol Toxicol Methods 2010;61:205–9.
22. Kim MP, Evans DB, Wang H, Abbruzzese JL, Fleming JB, Gallick GE. Generation of orthotopic and heterotopic human pancreatic cancer xenografts in immunodeficient mice. Nat Protoc 2009;4:1670–80.
23. Liau SS, Whang E. HMGA1 is a molecular determinant of chemoresistance to gemcitabine in pancreatic adenocarcinoma. Clin Cancer Res 2008;14:1470–7.
24. Larbouret C, Robert B, Bascoul-Mollevi C, Penault-Llorca F, Ho-Pun-Cheung A, Morisseau S, et al. Combined cetuximab and trastuzumab are superior to gemcitabine in the treatment of human pancreatic carcinoma xenografts. Ann Oncol 2010;21:98–103.
25. Casadonte R, Caprioli RM. Proteomic analysis of formalin-fixed paraffin-embedded tissue by MALDI imaging mass spectrometry. Nat Protoc 2011;6:1695–709.
26. Kasuya K, Tsuchida A, Nagakawa Y, Suzuki M, Abe Y, Itoi T, et al. Hypoxia-inducible factor-1alpha expression and gemcitabine chemotherapy for pancreatic cancer. Oncol Rep 2011;26:1399–406.
27. Onozuka H, Tsuchihara K, Esumi H. Hypoglycemic/hypoxic condition in vitro mimicking the tumor microenvironment markedly reduced the efficacy of anticancer drugs. Cancer Sci 2011;102:975–82.
28. Zhao X, Gao S, Ren H, Sun W, Zhang H, Sun J, et al. Hypoxia-inducible factor-1 promotes pancreatic ductal adenocarcinoma invasion and metastasis by activating transcription of the actin-bundling protein fascin. Cancer Res 2014;74:2455–64.
29. Jones L, Ghaneh P, Humphreys M, Neoptolemos JP. The matrix metalloproteinases and their inhibitors in the treatment of pancreatic cancer. Ann N Y Acad Sci 1999;880:288–307.
30. Merdad A, Karim S, Schulten HJ, Dallol A, Buhmeida A, Al-Thubaity F, et al. Expression of matrix metalloproteinases (MMPs) in primary human breast cancer: MMP-9 as a potential biomarker for cancer invasion and metastasis. Anticancer Res 2014;34:1355–66.
31. Yang X, Staren ED, Howard JM, Iwamura T, Bartsch JE, Appert HE. Invasiveness and MMP expression in pancreatic carcinoma. J Surg Res 2001;98:33–9.
32. Kunjithapatham R, Geschwind JF, Rao PP, Boronina TN, Cole RN, Ganapathy-Kanniappan S. Systemic administration of 3-bromopyruvate reveals its interaction with serum proteins in a rat model. BMC Res Notes 2013;6:277.
33. Schaefer NG, Geschwind JF, Engles J, Buchanan JW, Wahl RL. Systemic administration of 3-bromopyruvate in treating disseminated aggressive lymphoma. Transl Res 2012;159:51–7.
34. Zhang J, Ma PX. Cyclodextrin-based supramolecular systems for drug delivery: recent progress and future perspective. Adv Drug Deliv Rev 2013;65:1215–33.
35. Heidel JD, Schluep T. Cyclodextrin-containing polymers: versatile platforms of drug delivery materials. J Drug Deliv 2012;2012: 262731.
36. Guillaumond F, Leca J, Olivares O, Lavaut MN, Vidal N, Berthezene P, et al. Strengthened glycolysis under hypoxia supports tumor symbiosis and hexosamine biosynthesis in pancreatic adenocarcinoma. Proc Natl Acad Sci U S A 2013;110:3919–24.
37. Cao X, Jia G, Zhang T, Yang M, Wang B, Wassenaar PA, et al. Noninvasive MRI tumor imaging and synergistic anticancer effect of HSP90 inhibitor and glycolysis inhibitor in RIP1-Tag2 transgenic pancreatic tumor model. Cancer Chemother Pharmacol 2008;62: 985–94.
38. Xiao H, Li S, Zhang D, Liu T, Yu M, Wang F. Separate and concurrent use of 2-deoxy-D-glucose and 3-bromopyruvate in pancreatic cancer cells. Oncol Rep 2013;29:329–34.
39. Xu RH, Pelicano H, Zhou Y, Carew JS, Feng L, Bhalla KN, et al. Inhibition of glycolysis in cancer cells: a novel strategy to overcome drug resistance associated with mitochondrial respiratory defect and hypoxia. Cancer Res 2005;65:613–21.
40. Matsumoto S, Saito K, Yasui H, Morris HD, Munasinghe JP, Lizak M, et al. EPR oxygen imaging and hyperpolarized 13C MRI of pyruvate metabolism as noninvasive biomarkers of tumor treatment response to a glycolysis inhibitor 3-bromopyruvate. Magn Reson Med 2013;69: 1443–50.
41. Mollenhauer J, Roether I, Kern HF. Distribution of extracellular matrix proteins in pancreatic ductal adenocarcinoma and its influence on tumor cell proliferation *in vitro*. Pancreas 1987;2: 14–24.
42. Longati P, Jia X, Eimer J, Wagman A, Witt MR, Rehnmark S, et al. 3D pancreatic carcinoma spheroids induce a matrix-rich, chemoresistant phenotype offering a better model for drug testing. BMC Cancer 2013;13:95.
43. Ganapathy-Kanniappan S, Kunjithapatham R, Torbenson MS, Rao PP, Carson KA, Buijs M, et al. Human hepatocellular carcinoma in a mouse model: assessment of tumor response to percutaneous ablation by using glyceraldehyde-3-phosphate dehydrogenase antagonists. Radiology 2012;262:834–45.
44. Schneiderhan W, Scheler M, Holzmann KH, Marx M, Gschwend JE, Bucholz M, et al. CD147 silencing inhibits lactate transport and reduces malignant potential of pancreatic cancer cells in in vivo and in vitro models. Gut 2009;58:1391–8.
45. Shih HJ, Chen HH, Chen YA, Wu MH, Liou GG, Chang WW, et al. Targeting MCT-1 oncogene inhibits Shc pathway and xenograft tumorigenicity. Oncotarget 2012;3:1401–15.
46. Sonveaux P, Copetti T, De Saedeleer CJ, Vegran F, Verrax J, Kennedy KM, et al. Targeting the lactate transporter MCT1 in endothelial cells inhibits lactate-induced HIF-1 activation and tumor angiogenesis. PLoS ONE 2012;7:e33418.

Published OnlineFirst October 17, 2014; DOI: 10.1158/1078-0432.CCR-14-1271

Clinical Cancer Research

Systemic Delivery of Microencapsulated 3-Bromopyruvate for the Therapy of Pancreatic Cancer

Julius Chapiro, Surojit Sur, Lynn Jeanette Savic, et al.

Clin Cancer Res 2014;20:6406-6417. Published OnlineFirst October 17, 2014.